Numerical Simulation of Intense Reaction Propagation in Multiphase Systems

Ronald Pape
Explosion Science Section, IIT Research Institute, Chicago, IL 60616

Dimitri Gidaspow
Dept. of Chemical Engineering, Illinois Institute of Technology, Chicago, IL 60616

A numerical model was evaluated including Arrhenius reaction kinetics to simulate multiphase flows with intense reactions and severe property gradients. Although these problems are common in chemical engineering, such an extreme case as detonation propagation in a dispersed particulate flow was investigated. The model was evaluated with respect to the form of the conservation relations being simulated, frame invariance verification, constitutive relations, numerical stability, numerical diffusion, and model verification using available experimental results and equilibrium thermochemical predictions. The model was adequate with respect to numerical issues of particular concern such as stability and numerical diffusion. To simulate experimental results realistically, Arrhenius reaction kinetics alone were insufficient. When considering important physical mechanisms in the reaction modeling based on single particle heat transfer, the multiphase model simulates experimental results realistically.

Introduction

Multiphase reactive flow modeling has application in a wide variety of chemical engineering problems. The most obvious application is simulation of chemical reactors in which the interaction of different phases controls or has strong influence on the rate of reaction. Fluidized-bed reactors are a subset of multiphase reactive flows. Combustion problems are characterized by interaction of condensed and gaseous phases, and tracking of gas-phase components which mix and react. Dust explosions can involve deflagration and detonation phenomena. Detonation problems in multiphase systems represent an extreme situation in multiphase reactive flow simulation. All the elements of multiphase flow are involved in such simulations, but in addition detonation problems challenge simulation models to the extreme with respect to reaction rates and the existence of discontinuities such as fluid dynamic shocks. It is for this reason that detonation establishment in a multiphase reactive flow is considered to be an excellent platform for developing an understanding of the limitations in the numerical modeling of multiphase reactive flows. Particular issues that should be addressed in such numerical analyses include: the form of the conservation relations being simulated, frame invariance, constitutive relations, numerical stability, numerical diffusion, effect of numerical cell size, and model verification. This article provides a forum for discussion of these issues that must be addressed in numerical analysis.

A particular multiphase numerical model will be described and evaluated. This is the code of Gidaspow and his associates at the Illinois Institute of Technology, as described in Wu and Gidaspow (1997), Pape et al. (1996a,b), Gidaspow (1994), Gidaspow et al. (1984), Sun et al. (1994), Aldis (1987), Aldis and Gidaspow (1990), and Lyczkowski et al. (1978). As a test case to challenge the model to extremes of reaction rate and fluid dynamic discontinuities, IIT Research Institute detonation tube experiments are numerically simulated. IIT Research Institute detonation tube experimental results have been presented in Tulis and Sumida (1994), Tulis and Selman (1982), Tulis et al. (1983), Tulis et al. (1990, 1991, 1994), and other publications. The simulation results are compared to experimental data and Chapman-Jouguet detonation characteristics as predicted by an equilibrium thermochemical code, TIGER of Cowperthwaite and Zwisler (1984). It was necessary to apply the results of a single particle heat transfer and reaction model in order to obtain a good simulation of experimental measurements.

One-dimensional analyses were done to determine the effects of particulate concentration, initiation source intensity, and Arrhenius reaction rate. The establishment of stable det-

onation propagation in a detonation tube experimental facility was simulated in two dimensions for RDX explosive in particulate form at 1.6 kg/m^3 average concentration, and predictions compared well with observed experimental results for this case. To investigate this problem, simulations for a long tube were done with increased axial grid size. The model predicts a stable shock front followed by an attenuating pressure surge which appears to be due to pressure reflections within the tube induced by the initiation source.

Model Description

A multiphase computational fluid dynamics computer code has been used at the Illinois Institute of Technology for a number of years to investigate a wide variety of problems from fluidized-bed flow to electrostatic separation. There was a recent investigation of a fluidized bed with reaction by Wu and Gidaspow (1997), but the reaction rates were not severe in that simulation, as discussed in Pape et al. (1996a). Much of the ongoing development at the Illinois Institute of Technology is emphasizing development and application of the kinetic theory of granular solids to provide a more realistic prediction of transport within the particulate phases. The analyses presented in this article did not employ the kinetic theory. The multiphase model and kinetic theory of granular solids are described in depth by Gidaspow (1994). A comprehensive discussion of the governing equations and constitutive relations is provided in that reference, as well as in several articles describing the model (Wu and Gidaspow, 1997; Gidaspow et al., 1984; Sun et al., 1994).

The computer program that was used was originally developed by Rivard and Torrey (1977) as the K-FIX code, an extension of the numerical method developed by Harlow and Amsden. This code has evolved significantly over the years as it has been adapted to a wide variety of applications. The most similar work to that presented herein was by Aldis (1987) and Aldis and Gidaspow (1990). Aldis applied a revised version of the code, MULTIP, with a pressure law reaction rate to simulate combustion propagation in a packed bed of propellant and a dispersed explosive system. The work done at that time has been extended or modified in several significant aspects. Instead of using a pressure law to represent the reaction kinetics, Arrhenius kinetics were used in the present study. Aldis used the energy form of the conservation of energy equation and the current work uses the conservation of enthalpy form. In Aldis and Gidaspow (1990), the Model A form described in Gidaspow (1994) was used. Models A and B differ in that Model B considers no pressure drop applied to the particulate phases. The Model A form has terms involving the time rate of change and transport of the void fraction, and those terms are not present here. Lyczkowski et al. (1978) showed that the Model A form is ill-posed, and numerical anomalies could result. The current model is based on the Model B form of the equations, which has been shown to be well posed by Lyczkowski et al. (1978).

The model equations are presented in Table 1. The constitutive equations that close the solution are discussed in depth in several other works: Pape (1996), Pape et al. (1996a,b), Gidaspow (1994), and Sun et al. (1994). The constitutive relations will not be presented in detail here, but several terms warrant some additional discussion.

Table 1. Model Equations

Conservation of Mass of Phase K

$$\frac{\partial(\epsilon_k \rho_k)}{\partial t} + \frac{1}{R}\nabla\cdot(R\epsilon_k \rho_k \upsilon_k) = \dot{m}_k \quad (1)$$

Conservation of Momentum for the Continuous Fluid Phase

$$\frac{\partial(\epsilon_f \rho_f \vec{v}_f)}{\partial t} + \frac{1}{R}\nabla\cdot(R\epsilon_f \rho_f \vec{v}_f \vec{v}_f) = -\nabla p_f + \sum_k \beta_{kf}(\vec{v}_k - \vec{v}_f) + \nabla\cdot\epsilon_f\overline{\overline{T}}_f + \epsilon_f \vec{g} + \dot{m}_f \vec{v}_f^{*}. \quad (2)$$

Conservation of Momentum for the Condensed Phases

$$\frac{\partial(\epsilon_k \rho_k \vec{v}_k)}{\partial t} + \frac{1}{R}\nabla\cdot(R\epsilon_k \rho_k \vec{v}_k \vec{v}_k) = \beta_{fk}(\vec{v}_f - \vec{v}_k) - G\nabla\epsilon_k + \nabla\cdot\epsilon_k\overline{\overline{T}}_k + (\rho_k - \rho_f)\epsilon_k \vec{g} + \dot{m}_k \vec{v}_k^{*} \quad (3)$$

Enthalpy Form of the Conservation of Energy

Fluid Phase

$$\frac{\partial}{\partial t}(\epsilon_f \rho_f H_f) + \frac{1}{R}\nabla\cdot(R\epsilon_f \rho_f H_f \upsilon_f) = \left(\frac{\partial p_f}{\partial t} + \upsilon_f\cdot\nabla p_f\right) + \Phi_f + \sum_k h_{fk}(T_k - T_f) + \sum_k \beta_{fk}(\upsilon_k - \upsilon_f)^2 + \frac{1}{R}\nabla\cdot(Rk_f\nabla T_f) + \dot{m}_f \Delta H_f \quad (4)$$

Solid Phases

$$\frac{\partial}{\partial t}(\epsilon_k \rho_k H_k) + \frac{1}{R}\nabla\cdot(R\epsilon_k \rho_k H_k \upsilon_k) = \sum_k h_{fk}(T_f - T_k) + \frac{1}{R}\nabla\cdot(Rk_k\nabla T_k) + \Phi_k + \dot{m}_k \Delta H_k \quad (5)$$

Volume Fractions Sum to Unity

$$\epsilon_f + \sum_k \epsilon_k = 1 \quad (6)$$

The ideal gas law was used for the majority of simulations presented in this article. The Redlich-Kwong equation of state was used in some cases, but it was determined that at the pressure levels encountered in the cases evaluated (generally less than 100 bar), the ideal gas law was sufficient.

The specific heat of the gas phase was computed using the power law expression given in Smith and Van Ness (1987)

$$\frac{C_{p_i}^{ig}}{R} = A_i + B_i T + C_i T^2 + D_i T^{-2} \text{ and } C_{p_{\text{mixture}}}^{ig} = \sum_i y_i C_{pi}^{ig} \quad (7)$$

with the coefficients A_i, B_i, C_i, and D_i given for a variety of pure chemical species i.

There is a term in the momentum equations (Eqs. 2 and 3 in Table 1) that accounts for the contribution to momentum due to mass transfer between phases. This term was handled differently here than it was handled in Aldis (1987) and Aldis and Gidaspow (1990), as well as a number of other works. The form of that term has a major effect on (for example) the detonation front velocity, and the current form is based on physical reasoning that is consistent with the detonation propagation problem.

For example, for the case of a detonation propagating into a dispersed solid explosive cloud, the unreacted phases are at essentially zero velocity before the detonation shock front arrives. When the shock front crosses into the unreacted medium, it is followed by product gases and other constituents at high velocities. The different phases at the location of intense reaction are at vastly different velocities. Us-

ing the wrong starred velocity in Eqs. 2 and 3 can lead to serious errors in the shock propagation velocity. Physical reasoning should be used to determine the appropriate starred velocity to use in each case. The term $\dot{m}_f \vec{v}_f^*$ in the gas-phase momentum equation is the momentum due to the generation of gas (from reaction) which is added to the fluid element at some velocity. It is important to recognize that the relevant velocity is that of the source of the gas being added. In the case of detonation propagation within a dispersed explosive cloud, the source of the gas being added is from the particulate phases. Therefore, in the gas momentum equation, v_f^* is the velocity of the particles themselves, mass averaged to appropriately represent the overall gas generation. Conversely, in the solids momentum equations, the particles are losing mass at the particles' velocities. Therefore, in the solids momentum equations, the appropriate velocities are V_k. This is an important distinction for the detonation problem, but may not be nearly as important in many other systems. When the proper source velocity is not accounted for in the computations, serious errors can result.

Powers et al. (1990) used the same form of this term as is used here. They indicate that by applying the Galilean transformation to the equations, it can be shown that the form is invariant with respect to the frame of reference as required. Frame invariance is demonstrated for the momentum equations in the Appendix to this article. It is interesting to note that the analysis in the Appendix shows that in order to demonstrate frame invariance, the source velocity can be any velocity. The term must be present to demonstrate frame invariance, but from a practical standpoint the source velocity can be zero. In the dispersed explosive detonation problem, the solids velocity is nearly zero at the time the pressure front moves over the unreacted particles. If the reaction occurs quickly, the source velocity can be essentially zero in the system.

The solids viscosity used in this work was that of Miller and Gidaspow (1992).

$$\mu_k = 5\epsilon_k \quad \text{poise} \tag{8}$$

This expression used for solids viscosity was based on experimental data for a fluidized bed. The expression may not be appropriate for strong shear flow and severe property gradients that are experienced locally in detonation problems. Major improvements in the prediction of the solids viscosity have been made more recently at IIT by Gidaspow and Huilin (1996).

Single particle modeling

The relations presented above are those used in the multiphase computer code being evaluated. The multiphase code heats the particles in the flow by convection assuming that the individual particles heat up at a uniform internal temperature, that is, effectively, the particles are of infinite thermal conductivity and have no temperature gradient within the individual particles. For many problems, this assumption is adequate, but when heating is intense, there is likely to be a significant temperature profile within the particles. With a temperature profile inside a particle, the reaction consumption of the particle is likely to be significantly different than if the temperature were constant within the particle. To assess this effect, a single particle reaction model was developed. A single spherical RDX explosive particle was modeled numerically to predict the reaction duration. Two cases were considered: a particle with a constant internal temperature (constant spatially but transient) and a particle with a finite conduction and consequent radial temperature profile. For the particle with finite conduction, the particle radius decreased as material was consumed in reaction, that is, surface regression was included. For the conductive particle, the following model was considered

$$\frac{\partial T}{\partial t} - \alpha \frac{1}{r^2} \frac{\partial}{\partial r}\left(r^2 \frac{\partial T}{\partial r}\right) = \frac{Q_o}{\rho C_p} \exp\left(-\frac{E}{\Re T}\right) \tag{9}$$

where T is temperature, t is time, α is molecular diffusivity of heat, r is radial distance, $Q_o = \Delta H \rho Z$, ΔH is enthalpy increase due to reaction, ρ is material density, Z is the Arrhenius pre-exponential factor, C_p is specific heat, E is activation energy, and $\Re$ is gas constant. This equation was modeled with a regressing particle surface and compared to the equivalent constant temperature particle model. In both cases, a convective boundary condition was applied with Nusselt Number and temperature of the surroundings corresponding to the Chapman-Jouguet detonation state as predicted using the TIGER code (Cowperthwaite and Zwisler, 1984). The ratio of reaction times predicted from the single particle model with finite conduction to reaction times predicted from the single particle constant temperature model are plotted in Figure 1. Clearly, reaction times can be quite different than predicted with the constant particle temperature approach. As shown later, accounting for the reaction delay due to heat transfer significantly improves prediction of detonation using the multiphase model.

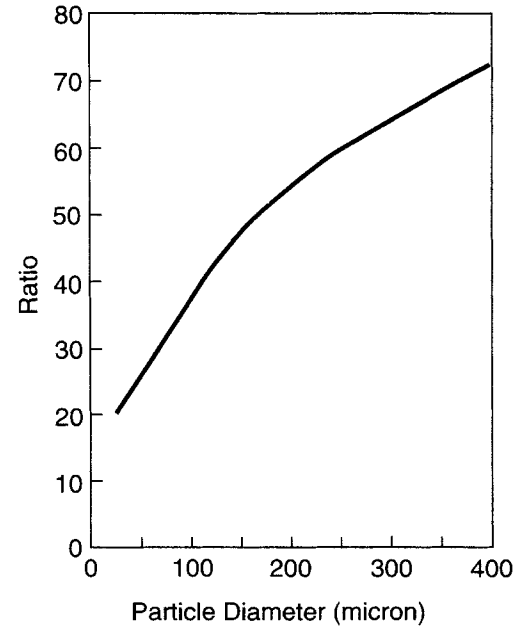

Figure 1. Ratio of reaction times from single particle conduction model to constant temperature model.

Numerical Issues

Numerical scheme

The numerical scheme used in the IIT code is the implicit continuous Eulerian (ICE) approach. The model uses donor cell differencing. The conservation of momentum and energy equations are in mixed implicit-explicit form. With respect to the convection and reaction terms, the momentum equations are fully explicit. The continuity equations excluding mass generation are implicit form.

Numerical stability

The stability analysis discussed in this section was presented previously in Pape et al. (1996a). A stability analysis was conducted on the finite difference form of the continuity, momentum and energy equations. To illustrate the method, the continuity equation will be discussed, however, with some parameter modifications the method and general results obtained apply to the momentum and energy equations as well. The continuity equation is repeated here in Eq. 10.

$$\frac{\partial(\epsilon_k \rho_k)}{\partial t} - \nabla(\epsilon_k \rho_k v_k) = \dot{m}_k \tag{10}$$

The finite difference form of the continuity equation in 2-D Cartesian coordinates in the code being evaluated is

$$(\epsilon_k \rho_k)_{i,j}^{n+1} = (\epsilon_k \rho_k)_{i,j}^{n} - \frac{\delta t}{\delta x_i}\langle(\epsilon_k \rho_k)u_k\rangle_{i,j}^{n+1} - \frac{\delta t}{\delta y_j}\langle(\epsilon_k \rho_k)v_k\rangle_{i,j}^{n+1} + \delta t \dot{m}_{k_{i,j}}^{n} \tag{11}$$

where δx and δy are the spatial increments, δt is the time increment, i and j are spatial indices, and n is the time increment. The bracket $\langle\rangle$ notation symbolizes net flux of the bracketed property into and out of the cell. The mass generation term can be represented in the following form

$$\dot{m}_{k_{ij}}^{n} = (\epsilon_k \rho_k)_{ij}^{n} Z_k \exp\left[-\frac{E_k}{\Re T_{k_{ij}}^{n}}\right] = (\epsilon_k \rho_k)_i^{n} M \tag{12}$$

where $\Re$ is the gas constant, E_k is the activation energy for the phase k reaction, and Z_k is the preexponential factor for the phase k reaction. In the analyses that follow, the preexponential factor Z_k times the exponential term is denoted M and is taken as a constant in this stability analysis. In reality this term is a strong function of temperature. In the current analysis, by identifying a limit for M, a maximum allowable temperature is identified that must not be exceeded in order to maintain stability.

In order to simplify the analysis, we consider one dimension with constant spatial increment δx and constant time step δt. It is also assumed that all velocities are in the positive x direction corresponding to a specific donor cell differencing configuration.

The donor cell flux term in the continuity equation is given by the following equation:

$$\langle(\epsilon_k \rho_k)v_k\rangle_i^{n+1} = v_{k,i+(1/2)}^{n+1}(\epsilon_k \rho_k)_i^{n+1} - v_{k,i-(1/2)}^{n+1}(\epsilon_k \rho_k)_{i-1}^{n+1} \tag{13}$$

Velocity will be taken as a constant U and we define the following parameters

$$F_i' = F_i^{n+1} = (\epsilon_k \rho_k)_i^{n+1} \tag{14}$$
$$F_i = F_i^{n}$$
$$R = \frac{\delta t}{\delta x}$$

Notice that the product RU is the well-known Courant parameter. With substitution of parameters, the continuity equation becomes

$$F_i' = F_i - RU(F_i' - F_{i-1}') + M\delta t F_i \quad \text{(Mixed Explicit-Implicit)} \tag{15}$$

Although this is the form of the conservation of mass equation in the code being assessed, in principle the formulation alternately could be fully explicit or fully implicit

$$F_i' = F_i - RU(F_i - F_{i-1}) + M\delta t F_i \quad \text{(Fully Explicit)} \tag{16}$$

$$F_i' = F_i - RU(F_i' - F_{i-1}') + M\delta t F_i' \quad \text{(Fully Implicit)} \tag{17}$$

Each of these forms was analyzed by applying a Von Neumann stability analysis. Separation of variables is accomplished by assuming F to be of the form

$$F_i^n = \lambda^n e^{iJ\theta} \tag{18}$$

where λ^n accounts for variation with time and $e^{iJ\theta}$ accounts for spatial variations.

Using this assumed form in the various model equations and solving for λ (the amplification factor), stability criteria are derived by observing that the magnitude of the amplification factor must be less than or equal to 1 for absolute stability ($|\lambda| \le 1$). Richtmeyer and Morton (1967) have noted that absolute stability may be too restrictive in some cases and growth of the solution (amplification) should be compared to the analytic solution instead, that is, for relative stability in our case $|\lambda| \le e^{M\delta t}$.

It was shown by Pape (1996) and Pape and Gidaspow (1996a) that the fully explicit numerical scheme is the most restrictive form with respect to numerical stability, therefore, only the fully explicit form will be discussed further at this time. For the fully explicit numerical scheme, a Von Neumann stability analysis leads to the following amplification factor for absolute stability

$$|\lambda| = [1 + 2(R^2U^2 - RU - RUM\delta t)(1 - \cos(\theta)) + M^2\delta t^2 + 2M\delta t]^{1/2} \tag{19}$$

with criteria

$$|\lambda| \le 1 \quad \text{(for absolute stability) and} \quad \frac{|\lambda|}{e^{M\delta t}} \le 1$$

(for relative stability) (20)

By plotting amplification factor as shown in Eqs. 19 or 20 vs. $M\delta t$ for different values of RU, the region of stability can be identified. Figure 2 is a plot of absolute and relative stability for the fully explicit scheme with reaction for the specific case of $RU = 0$. In all cases with the explicit scheme, absolute stability requires that $M\delta t$ be negative. When $RU = 0$ with relative stability, all positive values of $M\delta t$ have amplification factors less than or equal to 1, and are therefore stable. If either absolute or relative amplification factor is less than or equal to 1 in a range, the range will be stable. Figure 3 maps the bound of stability in the RU vs. $M\ \delta t$ plane. All values to the right of the curve are stable. The rectangle at the bottom has been selected as a practical bound. We chose the following bounds for computations

$$RU \le 0.5 \quad \text{(Modified Courant-Friedrichs-Lewy Criterion)} \tag{21}$$

$$|M\delta t| < 1 \tag{22}$$

For an Arrhenius type relation

$$M = Z_k \exp\left(-\frac{A_k}{T_k}\right), \quad \text{where} \quad A_k = \frac{E_k}{\mathfrak{R}}. \tag{23}$$

Typical values (RDX explosive) for E_k and Z_k are 2×10^5 J/mol and 3.162×10^{18} s^{-1}, respectively.

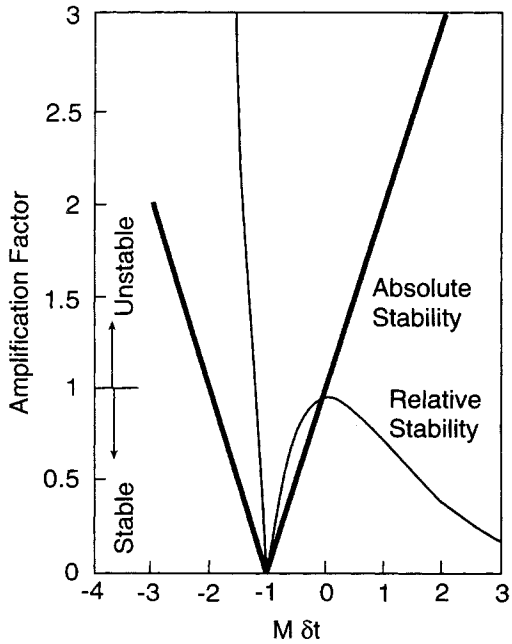

Figure 2. Stability for explicit form with reaction and *RU* = 0.

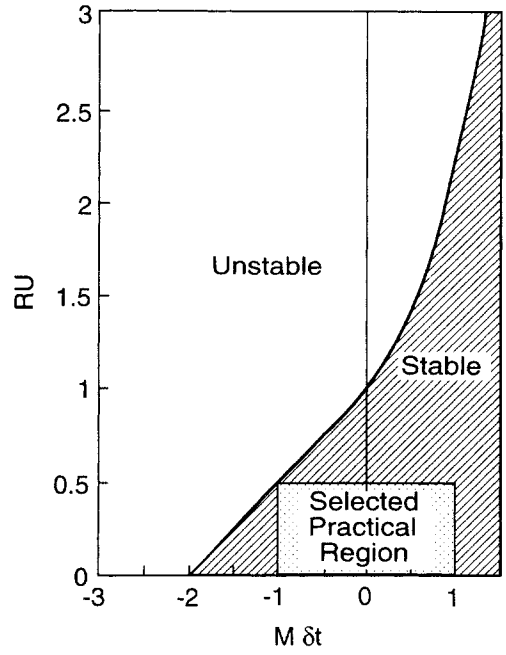

Figure 3. Stability map for fully explicit form.

Using the stability criteria given by Eqs. 21 and 22, a maximum temperature limit can be derived and imposed on the reaction to prevent instability. If the corresponding reaction rate is too low to numerically simulate the highest rates during the detonation, a significant error could be introduced. This should be tested by conducting simulations at several δt values with their corresponding critical temperature limits. For a specific δt value, the maximum temperature is given by

$$T_k = -\frac{A_k}{\ln\left(\frac{1}{z_k \delta t}\right)} \tag{24}$$

This approach was used in the setup of the numerical simulations presented in this article. It provides a logical scheme for selecting of parameters to avoid numerical instability.

Well-posedness of the system of equations is a subject closely aligned with stability analysis. It involves a matrix analysis of the system of conservation equations. If the system of equations is not well-posed, numerical instabilities can result and generate unrealistic results. The system of equations is well-posed if the equations are completely hyperbolic. Well-posedness is discussed in Gidaspow (1994), and the multiphase model has been analyzed by Lyczkowski et al. (1978) for two phases without reaction. Based on this analysis, it appears that the multiphase model with reaction should also be hyperbolic and well-posed, but the detailed analysis of the full system has not been done as yet.

Numerical diffusion

Numerical diffusion is a concern due to the occurrence of a fluid dynamic shock at a detonation front. Donor cell differencing is known to have significant numerical diffusion, and this could produce serious errors at the shock front.

Theory. The severity of the numerical problem can be evaluated by considering the form of the conservation equations and the numerics used to evaluate these equations. Consider the general form

$$L(M) = \frac{\partial M}{\partial t} + v\frac{\partial M}{\partial x} = 0 \tag{25}$$

where M is the parameter being conserved, such as ρ, ρv, or ρe. By considering the finite difference form of this equation with upwind donor cell differencing and applying Taylor series expansions in terms of x and t, the initial differential equation being evaluated can be expressed in the following form

$$\frac{\partial M}{\partial t} + v\frac{\partial M}{\partial x} = D\frac{\partial^2 M}{\partial x^2} \tag{26}$$

where the numerical diffusion is given by

$$D = \frac{1}{2}v\Delta x\left(1 - \frac{v\Delta t}{\Delta x}\right) \tag{27}$$

The second law of thermodynamics requires that the diffusion coefficient be positive, therefore, $v\Delta t/\Delta x$ must be less than or equal to 1. This is the Courant parameter. To minimize the numerical diffusion, the Courant parameter should be as close to 1 as possible, the velocity should be low or the spatial increment should be small. For the numerical simulations of detonation establishment near the initiation source described later in this article, this constraint was satisfied by using a small axial increment.

Numerical Experiments. To assess the severity of the numerical diffusion problem the multiphase code was used to simulate a shock tube for the configuration described in an article by Zha and Bilgen (1993) and an article by Van Leer (1979). The configuration is presented in Figure 4. The shock tube simulations were all one-dimensional. The high-pressure section of the shock tube initially contained 10 bar pressure of air at 300 K. The low-pressure side initially contained 1 bar at 300 K. The numerical cell size was 0.5 cm, the same as used in the Zha and Bilgen (1993) simulations. Several numerical schemes were evaluated in Zha and Bilgen (1993), including the Van Leer scheme. Van Leer developed and tested a second-order Godunov numerical procedure. Zha et al. developed a new flux vector splitting scheme and applied the scheme to the 1-D and multidimensional Euler equations. The 1-D shock tube problem was used as the basis for comparison of results with several numerical schemes including the Roe scheme, the Van Leer scheme, and the Liou-Steffen advection upstream splitting method. The multiphase code includes a number of terms not in the Euler equations. Therefore, the present simulations were not exactly analogous to the simulations using the Euler equations. However, numerical diffusion can be assessed for different codes by comparing the number of steps involved in the shock transition.

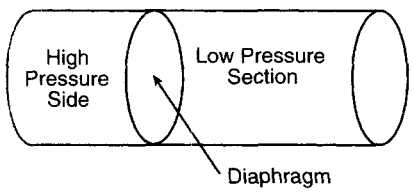

Figure 4. Shock tube configuration.

When considering pressure and density profiles at 0.1 s, all simulations presented in Zha and Bilgen (1993) involved approximately two to three numerical steps. These were simulations using their new flux vector splitting scheme as well as the other methods given above. The Van Leer (second-order Godunov) scheme required one to two steps to resolve the shock.

The multiphase code simulation for the pressure profile is given in Figure 5. The enthalpy form of the conservation of energy was used in this case. The shock pressure profile for the multiphase code requires three to five numerical steps. This was of comparable steepness to most of the methods tested in Zha and Bilgen (1993), although as just mentioned, some techniques such as the Van Leer method required only one to two steps. A code with high numerical diffusion can be compensated for by using a small spatial increment at the expense of a long run time and this was done in the majority of simulations reported herein.

This is not to imply that improvements would not be desirable. A considerable amount of work has been done over recent years to minimize numerical diffusion and dispersion in computational fluid dynamics codes. The Godunov et al. (1961) method and an improvement presented in Findlayson (1992) known as the random choice or Glimm's method are representative of the first category. The Van Leer method mentioned above was also in this category of numerical schemes. The second category of methods is known as flux corrected transport of FCT (see Baer and Gross, 1989; Baer et al., 1990; Book and Fry, 1984; Book, 1981; Boris and Book,

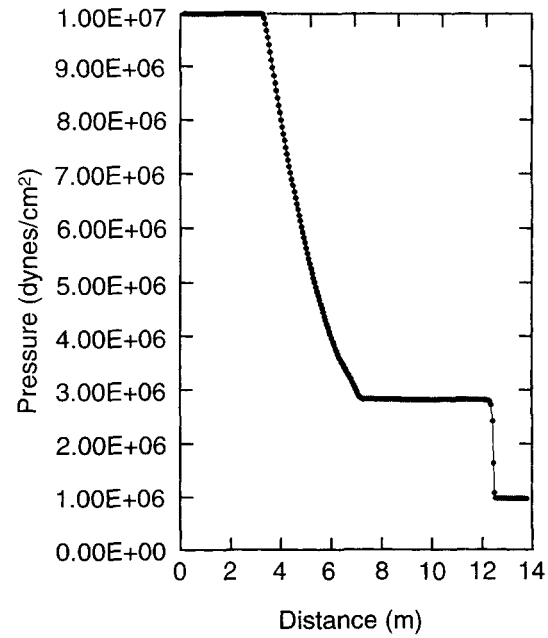

Figure 5. DTUBE pressure prediction for shock tube problem.

1976; Gross and Baer, 1985; Kunhardt and Wu, 1987) and extensions known as total variation methods, such as TVD (total variation diminishing) (see Chakravarthy et al., 1985; Chakravarthy and Osher, 1985; Yee, 1985; Yee, 1987).

Cell size effect

The size of the numerical grid can have an influence on accuracy. Numerical diffusion, which is related to the truncation error, was discussed in the last section. In addition, when sharp fluid dynamic discontinuities are present, reaction rates at these discontinuities are influenced by the thermodynamic state present. If the thermodynamic state (primarily temperature) is not correct, the reaction rates will be in error. The thermodynamic state is an average for each numerical grid. Small spatial increments allow better resolution of the thermodynamic state. At sharp discontinuities, averaging over a large numerical cell will result in peak values that are too low. For all of these reasons, cell size may have a significant influence and should be tested. Figure 6 shows peak pressure vs. axial increment for 2-D simulations of the detonation tube initiation process, close to the initiation source. The pressure plotted is the pressure just behind the detonation shock front. Three results are shown for simulations using a single particle size (22 micron). Extrapolation to zero axial increment indicates that the pressure should be slightly higher than 33 bar. Notice when a trimodal particle size distribution was used to better approximate Class 5 RDX explosive (the size distribution used in the experiments simulated), the predicted pressure would be somewhat higher, perhaps 36.5 bar. The particle-size distribution is a much more significant effect and should be accounted for.

Model Validation

This section presents the results of computer simulations that have been completed using the multiphase code to simulate development of detonation in the IIT Research Institute detonation tube for dispersed RDX explosive. Some of these results have been presented in Pape (1996) and Pape et al. (1996b) for determination of the distance required for the detonation front to stabilize in the tube.

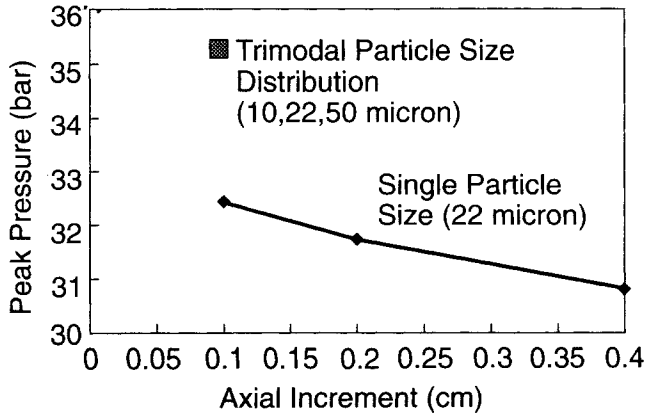

Figure 6. Effect of axial increment on peak pressure.

Detonation tube description

The IIT Research Institute has been conducting dispersed explosion research in a 15.24 cm dia. by 7.3 m (24 ft) long detonation tube experimental facility for the past 20 years. A great many formulations have been investigated in that facility and phenomena such as multiple front detonations and spinning detonations have been observed. The detonation tube is illustrated in Figure 7. The development of a stable detonation propagation in that system was chosen as a test case for evaluating a number of features of the multiphase reactive flow model. The development of stable propagation in the detonation tube is a good test case for several reasons. First, there is a considerable amount of experimental data available for comparison with numerical predictions. Second, the numerical model is challenged in terms of the intensity of the chemical reaction, and numerical stability issues can be assessed. Third, the development of stable detonation involves extreme property gradients associated with the shock at the detonation front, and numerical diffusion issues can be assessed.

As shown in Figure 7, the detonation tube facility consists of a disseminator cylinder, a solenoid valve, a tube leading from the disseminator to the main detonation tube, an instrumented section of the detonation tube, and an initiation explosive charge near the downstream end of the tube. The particulate energetic material to be tested is loaded into the disseminator cylinder. Typically, the load is about 200 g of material. A wide variety of materials have been tested, including aluminum powder, particulate explosives such as RDX, carbon, boron, ammonium nitrate oxidizer, and so on. These are dispersed in an appropriate oxidizing, reducing, or inert gaseous atmosphere. For example, RDX explosive has been tested in air and nitrogen. Ammonium nitrate has been dispersed in ethylene gas. As a test case, RDX explosive dispersed in air or nitrogen was selected for the work described in this article.

At the start of a test, the disseminator vessel is pressurized, typically at 200 psig (1,378 kPa). The solenoid valve is opened allowing the powder to flow through the disseminator tubing into the main detonation tube. The powder flows down the detonation tube creating what we believe to be a reasonably uniform particulate concentration profile within the test

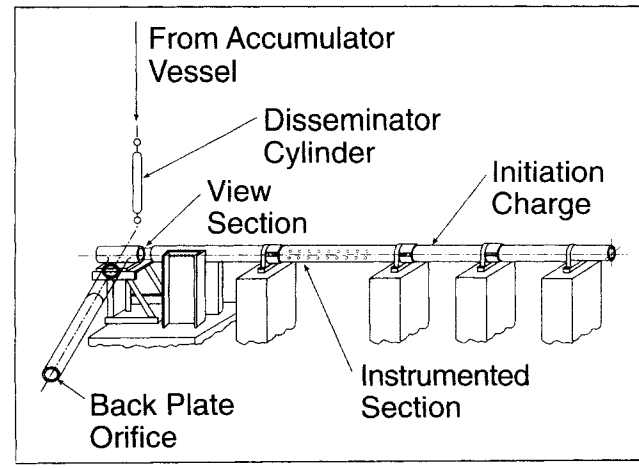

Figure 7. Detonation tube facility.

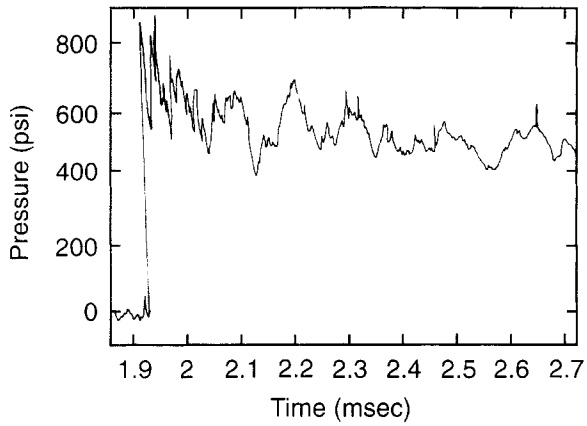

Figure 8. Typical pressure history from a detonation tube experiment with dispersed RDX explosive.

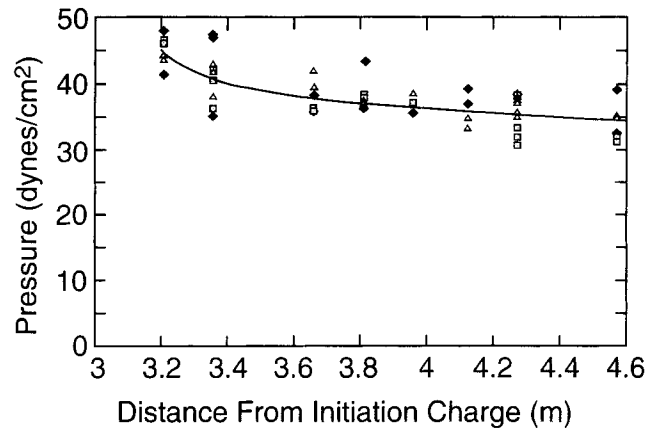

Figure 9. Pressure vs. distance for detonation tube experiments with RDX at 1.6 kg/m^3.

section. The dissemination process is timed such that a small initiating explosive charge is detonated just as the disseminator empties, and as the powder cloud just begins to flow out of the open back end of the detonation tube. The reaction begins to propagate radially outward from the initiating charge. It then travels back down the tube toward the disseminator as the reaction develops. Ultimately, it evolves into a stably propagating front, possibly a detonation.

Experimental data

A typical pressure trace for dispersed RDX tests is shown in Figure 8. Presenting the data on a condensed time scale reveals a classical exponential decay of the mean pressure. Whether the fluctuations about this mean are due to concentration nonuniformities, the instrumentation system, or some other phenomena, we believe that it is an average through these fluctuations that is meaningful for comparison with numerical simulations that assume a uniform concentration.

Table 2 summarizes results of early detonation tube experiments with dispersed RDX powder in nitrogen and air, as presented in Pape (1996). The values shown in the table are averages for all of the pressure gauges in the test section of the detonation tube. Based on more recent analysis of RDX-nitrogen test data, the peak pressures in Table 2 are believed to be high. Recent comprehensive analysis of data from six tests with RDX in nitrogen indicate that the average peak pressure is 41.5 bar, and the data asymptotes to 37.7 bar at the far end of the detonation tube.

When analyzing experimental data in the detonation tube, the data should be plotted as a function of distance down the tube. Figure 9 shows the experimentally derived peak pressure as a function of distance down the tube for three tests, which were presented in Pape et al. (1996b). Clearly, in these three tests the peak pressure decreases as the distance from the initiation source increases, and appears to asymptote to a steady level far down the tube. For the three tests plotted in Figure 9, the asymptote value is about 35 bar. For the recent tests mentioned above, the asymptote was 37.7 bar. The asymptote is the value that we believe should be compared to the predicted pressure just behind the shock front.

Table 2. Detonation Tube Experimental Data for Dispersed RDX

Avg. RDX Conc. (kg/m^3)	Peak Pres. (bar)	Detonation Velocity (m/s)	No. of Tests
0.8 (in air)	41.54	1,776	2
1.6 (in air)	57.46	2,037	2
1.6 (in nitrogen)	45.49	1,951	2

Equilibrium thermochemical code results

The TIGER Code of Cowperthwaite and Zwisler (1984) has been used to compute the Chapman-Jouguet detonation characteristics of RDX explosive at different concentrations in air and nitrogen. Results for RDX in air are presented here. The results for nitrogen are similar, but pressures were slightly lower. Figures 10 and 11 give the TIGER Code results. These results, as well as the experimental data, will be used later to help evaluate the multiphase code predictions.

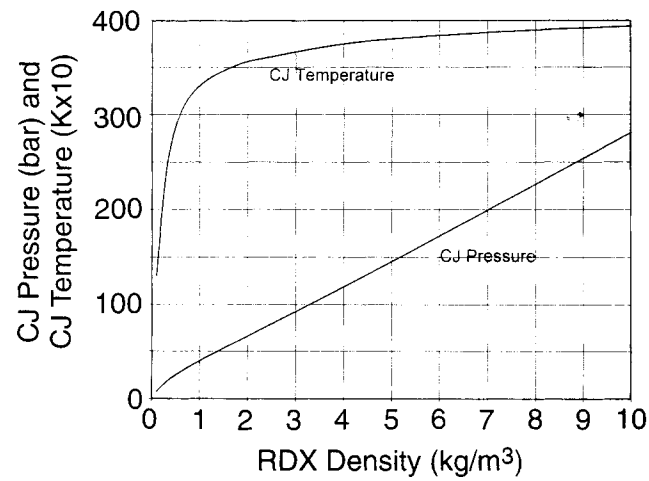

Figure 10. Tiger code predictions for RDX CJ pressure and temperature.

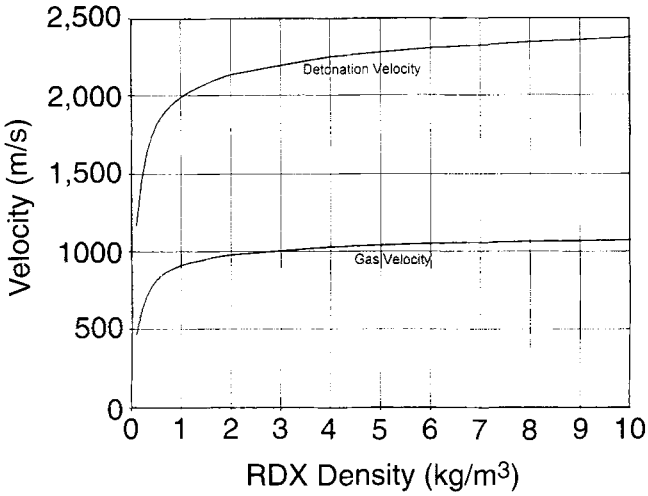

Figure 11. TIGER code predictions for detonation and gas velocities.

Numerical simulations

A great many computer simulations were completed in this work, and as the simulations progressed, more and more became apparent about model refinements required to achieve good simulation of experimental results. The model refinements that were assessed in this work included the form of the gas-phase specific heat, the form of the gas equation of state, and the model for heating the individual explosive particles in depth. The form of the gas equation of state was determined to be unimportant at the shock front in these simulations. The shock peak pressures were fairly low (generally below 100 bar) in the cases simulated, and the ideal gas law and the Redlich-Kwong equation of state gave essentially the same results for these conditions. The gas specific heat was a specified constant in the basic IIT code. This was determined to be inadequate for the detonation tube problems. A power series specific heat function of temperature significantly improved predicted results. By far the most significant finding, however, was that the particle heat transfer in the original IIT model was totally inadequate for the shock problem. The original model was based on the particles having constant internal temperature. The temperature gradient within the individual particles was not considered and it was found that the temperature within the individual particles must be accounted for. In the present work, the gas-particle heat transfer was adjusted based on the results of the single particle modeling to correct for the particle's internal temperature profile. This improved simulation results tremendously.

In the following sections, simulation results are summarized. The influences of a variety of parameters are discussed, including the most significant of the findings, mentioned above. Both 1-D and 2-D simulations of the establishment of detonation in a detonation tube have been conducted. Although the 1-D results do not demonstrate the full capabilities of the multiphase model, the 1-D simulations provide the clearest insight into the phenomena and model realism. The 1-D simulations considered the effects of RDX concentration, intensity of the initiation source, and the reaction rate. These results are quite informative phenomenologically. The 2-D simulations investigated the region near to the initiation explosive charge (initial development) and the establishment zone leading to stably propagating detonation far downstream (long tube simulations).

One-Dimensional Results. The first set of 1-D simulations considered the effect of explosive concentration. These simulations are summarized in Table 3. Concentrations of 0.4, 0.8, 1.6 and 3.2 kg/m^3 were assessed at two initiation intensities (2 and 15 bar). Initiation intensity did not make a significant difference here. The pressure histories are shown in Figure 12 for the weaker initiation stimulus (2 bar). Each case shown in the figure is a sequence of pressure profiles separated by a constant time increment. The simulations showed a quickly dying reaction at 0.4 kg/m^3. At 0.8 kg/m^3, the pressure front is a sharp spike that surges in intensity between 7 and 19 bar, whereas in limited experiments at 0.8 kg/m^3 (not presented here), stronger stable detonations were achieved. At 1.6 kg/m^3, the pressure profiles are no longer spiked. A broad plateau follows the shock front. These results indicate more difficulty to develop a stable detonation than was observed in experiments. These simulations did not include the correction for particle heating, and we believe that this accounts for the discrepency.

Table 4 evaluates the effect of initiation intensity. Three initiation intensities (pressure levels) were considered for two explosive concentrations levels. As indicated above when considering concentration effect, the initiation intensity appears to have little effect on the 1-D results.

Table 5 summarizes a series of 1-D simulations done to determine the effect of reaction rate. The Arrhenius preexponential factor Z was multiplied by the percent reduction indicated in each case. This effectively reduced the instantaneous reaction rate by that factor. The effects of these rate adjustments on detonation pressure, temperature, and deto-

Table 3. Effect of Explosive Concentration

Explosive Density (kg/m^3)	Initiation Source (bar)	Peak Pres. (bar)	Temp. (K)	Detonation Velocity (m/s)	Comments
0.4	2	decreasing 2.5–1.8	---	446	Drop to front
0.8	2	7–19	950–1,900	1,167	Spike front with pulsing amplitude
1.6	2	30.5	2,937	2,300	Plateau after front
0.8	15	8–19	1,800	1,125	Spike front with pulsing amplitude
1.6	15	31	2,900	2,344	Plateau after front
3.2	15	48.5	3,350	3,500	Plateau after front

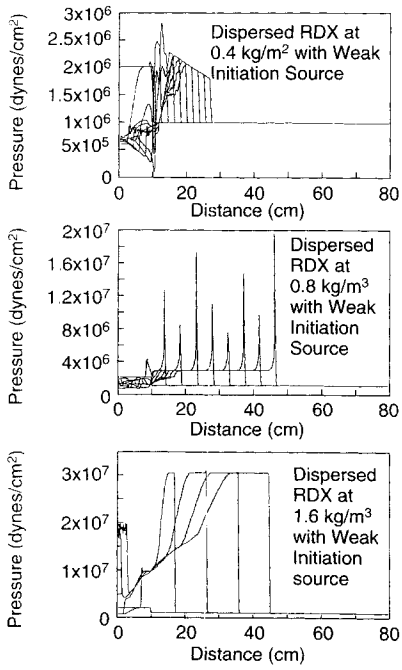

Figure 12. Effect of concentration on detonation development.

nation velocity are plotted in Figure 13. The effect of Arrhenius rate on pressure profiles is given in Figure 14. These effects of Arrhenius rate are considered by the authors to be significant, and this is directly related to the results of the single particle model presented earlier in this article. The single particle modeling (see Figure 1) showed that for a 22-micron particle (Class 5 RDX mean particle diameter) a more realistic analysis of the heat transfer inside the particle leads to a much slower reaction time than a particle model in which the particle temperature is constant with radius. For the 22 micron particle size, the correction factor was 20. Notice in Figure 13, when the reaction rate is slowed by a factor of 20, the pressure increases from 31 bar to about 35.8 bar. The temperature increases from 2,937 K to over 3,003 K, and the detonation velocity decreases from 2,300 m/s to 2,050 m/s. The results become more consistent with the experimental observations and TIGER code results when the single particle heat transfer is accounted for. Inclusion of a more realistic microscopic representation of the individual reactive particles with conduction or whatever realistically controls the reaction rate (mass transfer in a porous particle, physical particle breakup due to shock, and so on) could account for differences between the current model results and experiment.

Table 5. Effect of Arrhenius Rate

Adjustments to Arrhenius Rate	Explosive Density (kg/m^3)	Peak Pres. (bar)	Temp., (K)	Detonation Velocity (m/s)
0.5% Rate	1.6	58.32	2,971	1,850
1% Rate	1.6	50.9	2,992	2,000
5% Rate	1.6	35.8	3,003	2,050
20% Rate	1.6	32.1	2,976	2,250
Full Rate	1.6	30.5	2,937	2,300

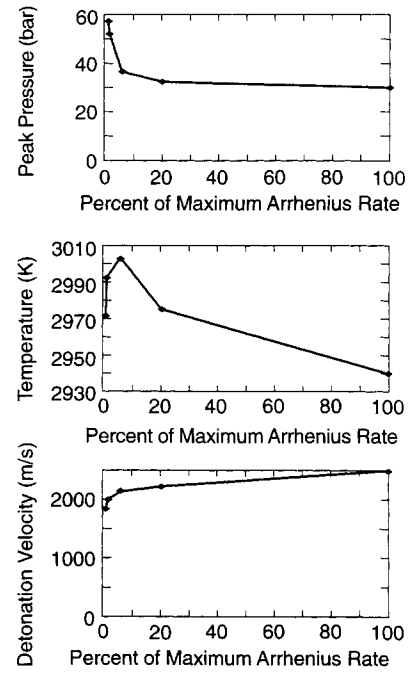

Figure 13. Effect of Arrhenius rate on detonation characteristics.

2-D Results. The initial 2-D simulations that were conducted used a fine numerical grid (primarily 0.1 cm in the axial direction with a few runs to assess the influence of axial grid size) concentrating on the region near to the initiation source. These were the initial simulations accomplished in support of the thesis research of Pape (1996). Color contour plots of pressure, temperature, and solids concentration were developed and animated in some cases. An example of a

Table 4. Effect of Initiation Source Intensity

Explosive Density (kg/m^3)	Initiation Source (bar)	Peak Pres. (bar)	Temp. (K)	Detonation Velocity (m/s)	Comments
0.8	2	7–19	950–1,900	1,167	Spike front with pulsing amplitude
0.8	2	7.5–15	---	1,000	Short run
0.8	15	8–19	1,800	1,125	Spike front with pulsing amplitude
1.6	2	30.5	2,937	2,300	Plateau after front
1.6	15	31	2,900	2,344	Plateau after front

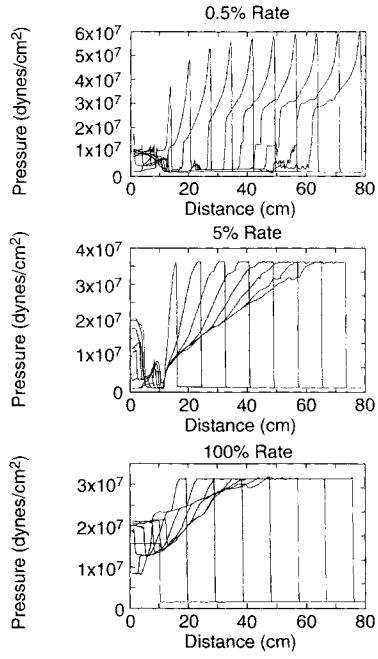

Figure 14. Effect of Arrhenius rate on pressure profiles.

pressure contour plot is given in Figure 15. The highest pressure levels are red (greater than 100 bar) and the lowest are blue (1-bar level) with the gradation of pressure between these limits going through the colors of the spectrum. Contour plots of this type reveal that there are pressure wave reflections off the tube walls that follow the shock front and contribute to a high-pressure surge that trails the shock front and attenuates as the event moves down the tube. This is made clearer in the long tube simulations discussed next.

The 2-D simulations of the establishment of detonation within a much longer distance down the length of the detonation tube were also completed. To compensate for the excessive computer running times on the DEC 5000 workstation used in this work, the long tube simulations were accomplished by increasing the numerical cell sizes. As the tube length was increased, the number of radial increments was minimized and the size of the axial increments was increased at the expense of some accuracy. Figure 16 shows pressure contour plots for a long tube run. The pressure profiles along the tube center line are shown in Figure 17. In the 800 cm long tube, the pressure surge following the shock front starts to rise again far from the initiator. It is believed that this is the start of a second pressure surge soon to start attenuating again, but this was not confirmed.

Comparison of Results to Experiment and Equilibrium Code Predictions

Results from the multiphase code predictions are compared to the TIGER equilibrium thermochemical code and experimental data in Table 6. The following observations can be made from the comparisons presented in the table:

- At 0.4 kg/m^3, the multiphase code predicts a dying event. The multiphase code predictions are considerably lower than those predicted by the equilibrium thermochemical code, and the pressure is decreasing with distance down the tube. It should be remembered that the equilibrium code starts with

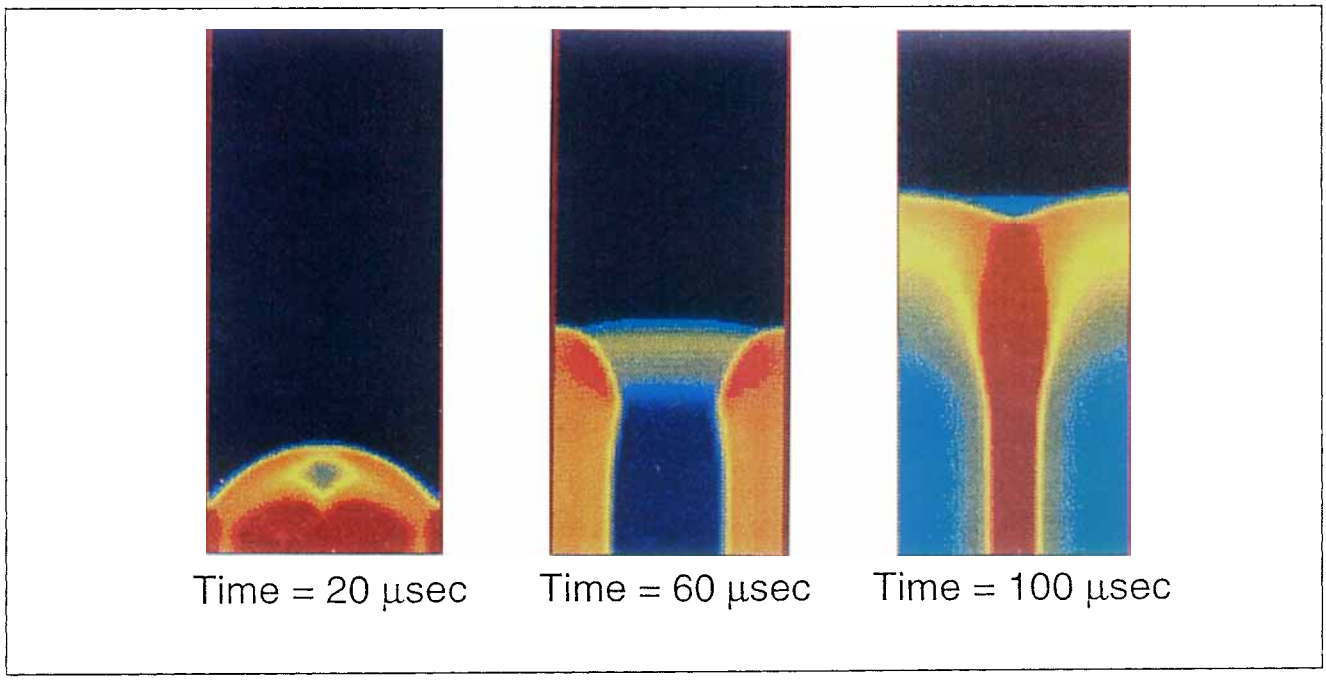

Figure 15. Pressure contour plot for initiation region.

Red areas are highest pressures and dark blue is ambient.

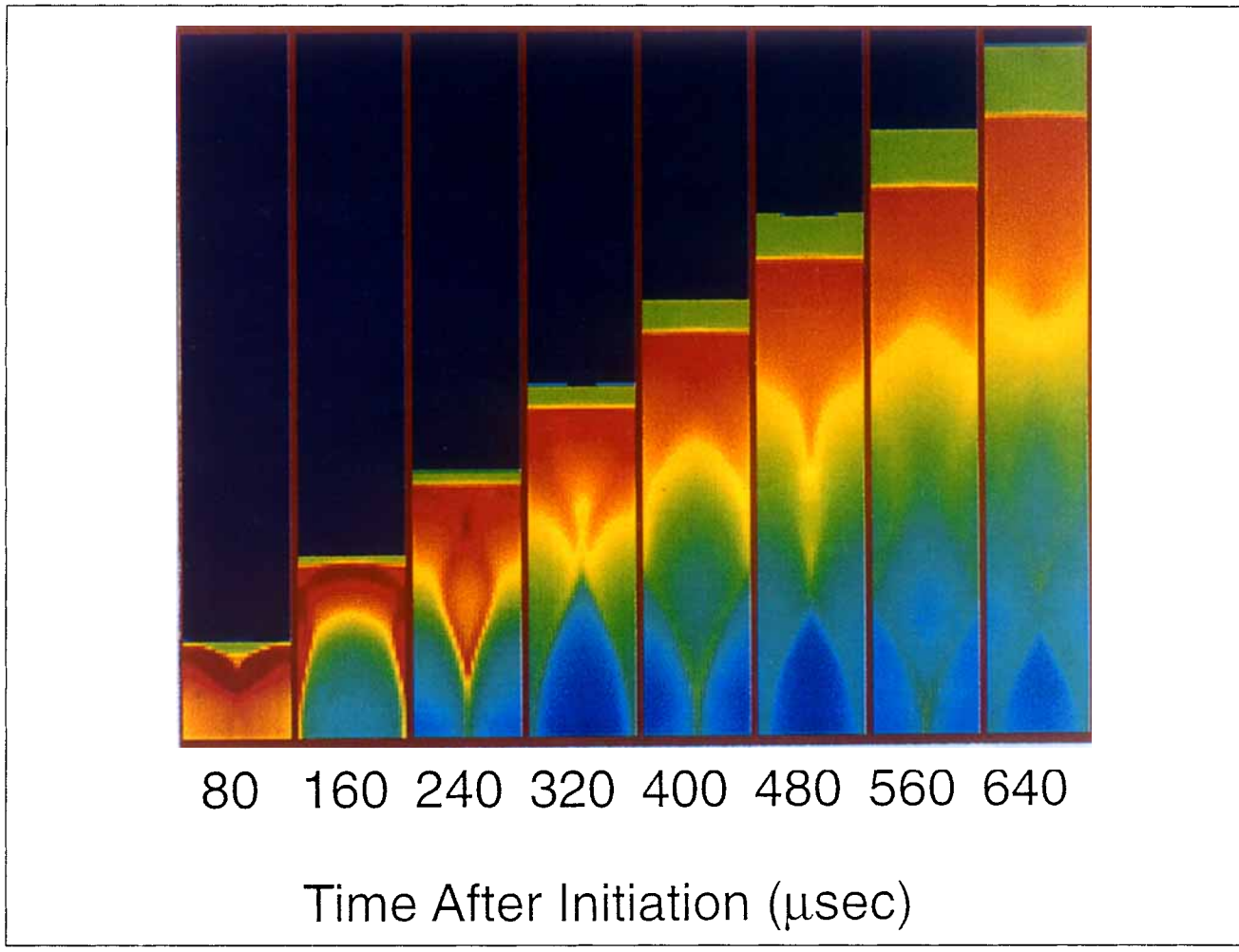

Figure 16. Pressure contour plot for long tube simulation.

the assumption that a fully stable detonation can propagate, and then computes the equilibrium thermodynamic state (pressure, temperature, and so on) that corresponds to that assumption. The multiphase code is nonequilibrium. It allows for reaction kinetics and nonideal effects. Unfortunately, there is no experimental data for comparison at 0.4 kg/m^3.

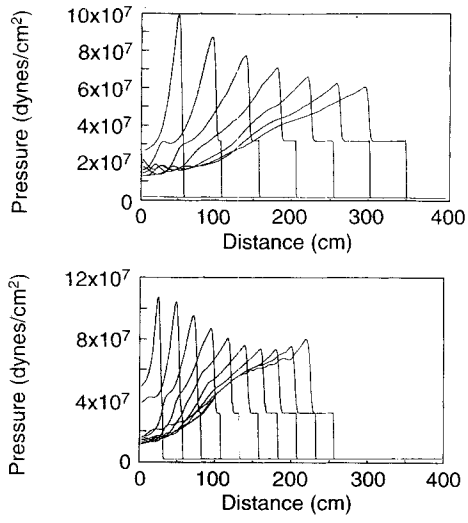

Figure 17. Pressure profiles for long tube simulations.

- At 0.8 kg/m^3, the multiphase code predicts what appears to be a borderline situation. A spiked pressure front is predicted to surge in amplitude as the detonation moves down the tube. Again predicted values are less than those predicted by the equilibrium code. The experimental data for this case is an average for all pressure gauges in the test section of the detonation tube. Pressure and detonation velocity in the experiment were higher than those predicted by the multiphase code.
- At 1.6 kg/m^3, the multiphase code predicts a stable detonation with pressure and detonation velocity comparable to the asymptotic experimental results at the far end of the test section. Although the comparison with experiment is fair, the predicted detonation front is slightly weaker (lower pressure and detonation velocity) than that observed in the experiments.
- At 1.6 kg/m^3, when the reaction rate is corrected to account for more realistic particle heating, there is excellent agreement with the experimental data for RDX in air ("rate corrected" blocks at 1.6 kg/m^3 in the table). The 5% rate correct was based on the single particle reaction modeling of a 22 micron RDX particle.

Table 6. Comparison of Results

RDX Density (kg/m^3)	Multiphase Code			Equilibrium Thermochemical Code*			Experimental Data			
	P (bar)	T (K)	D (m/s)	P (bar)	T (K)	D (m/s)	P (bar) Ave. of all peaks	P (bar) Asymp. at large dist.	(K)	(m/s)
0.4	2.5–1.8 (peak dying)	---	446	21.6	2,690	1,735	No Data	No Data	No Data	No Data
0.8	7–19 (surging peak)	950–1,900	1,125–1,167	34.1	3,191	1,934	41.54† (air)	---	No Data	1,757
1.6	31 (stable)	2,900	2,344	55.6	3,487	2,087	41.5 (N_2)	35–37.7** (N_2)	No Data	1,940 (N_2)
	35.8 (rate corrected)	3,003 (rate corrected)	2,050 (rate corrected)							
3.2	48.5 (stable)	3,350	3,500	97.72	3,500	2,200	No Data	No Data	No Data	No Data
	62.9 (rate corrected)	3,422 (rate corrected)	2,250 (rate corrected)							

*Equilibrium thermochemical code prediction *assumes* that stable steady propagation of detonation occurs.
**Values shown are asymptote values far downstream.
†Value based on limited data. Asymptote of values far downstream was not accounted for.

• At 3.2 kg/m^3, the multiphase code predicts a lower pressure and a higher detonation velocity than the equilibrium code. Although there is no experimental data for comparison at this concentration, we believe that the velocity predicted by the multiphase code with the full reaction rate is much too high at this concentration level. When the rate is slowed to 5% of the full rate, the multiphase code predictions are much more credible.

Conclusion

We believe that the critical factor in the modeling described in this article is the prediction of the reaction rate. The multiphase code uses Arrhenius kinetics with a simplified particle heat-transfer submodel based on uniform temperature inside the particles. It was shown that the temperature profile inside the particles must be accounted for to obtain good predictions of the detonation propagation. A factor to account for the effect of the internal temperature profile was derived based on single particle heat-transfer modeling. Figure 1 shows that accounting for the temperature profile within the explosive particles has a tremendous effect on the reaction time. For a 22-micron-dia. particle (average for Class 5 RDX), the reaction time is increased by a factor of about 20. Figure 13 shows (for 1.6 kg/m^3) that when the Arrhenius rate is slowed by this factor, the pressure and temperature increase while the detonation velocity decreases, producing a better match to the experimental results. These same trends also occur at the higher concentration level (3.2 kg/m^3), and better predictions appear to occur there also.

This work has identified an approach that we believe will result in significant additional improvements in predicted results. In nonequilibrium analyses such as the problems discussed in this article, modeling of the reaction rate can be quite important. For the detonation problem, it appears to be quite important to realistically model the rate controlling mechanisms. In this case, the rate controlling mechanism is the penetration of heat into the particle, which controls the Arrhenius decomposition rate in depth within the particle. Even the application of a simple factor derived from an independent single particle heat-transfer analysis provided good predicted results of detonation characteristics.

Notation

a = constant in gas conductivity temperature relation
b = exponent in gas conductivity temperature relation
C_D = drag coefficient
$C_{p_i}^{ig}$ = ideal gas specific heat of phase i
D = reference velocity in Galilean transfer
d_k = diameter for particles of phase k
e = coefficient of restitution for particle collisions
F = generalized quantity for stability analyses
g = gravitational acceleration
G = solid stress
h_{fk} = heat-transfer coefficient between fluid and phase k
H = enthalpy
H_k = enthalpy of phase k
k = thermal conductivity
k_{fo} = reference fluid conductivity
$\overline{M}_l$ = molecular weight of component l
Nu_k = Nusselt number for phase k heat transfer
P_f = fluid pressure
Pr = Prandtl number
$\hat{q}_k$ = particle-fluid convective heat transfer
R = coordinate factor (l for Cartesian and r for cylindrical coordinates)
R = stability parameter ($\Delta t/\Delta x^2$) in single particle model
Re_k = Reynolds' number for particles of phase k
S_k = conversion from area to volume basis for particles of diameter d_k

$\overline{\overline{T}}_k$ = stress tensor for phase k
T_k = temperature of phase k
T_0 = reference temperature for gas conduction relation
U_k = specific energy for phase k
$\vec{v}_k$ = velocity vector for phase k
v_r = radial velocity
v_z = axial velocity
X_I = induction distance
y_i = mole fraction of component i
z = axial distance
β_{kf} = fluid-particle friction coefficient
ΔH_k = enthalpy change in phase k due to reaction
ϵ_k = volume fraction of phase k
θ = granular temperature
λ = numerical stability amplification factor
μ = viscosity
ξ = distance variable in Galilean transform
ξ_k = bulk viscosity of phase k
ρ_k = density of phase k
$\overline{\overline{\tau}}_k$ = shear stress tensor for phase k
τ_I = induction time
φ = sphericity
Φ_k = energy dissipation rate for phase k
ϕ_k = sphericity of phase k

Subscripts

D = drag
f = fluid
i = spatial index in radial or x-Cartesian direction
I = induction
j = spatial index in axial or y-Cartesian direction
k = phase index
l = gas phase component index
o = reference value
r = radial direction

Literature Cited

Aldis, D. F., "Reactive Multiphase Hydrodynamics," PhD Thesis, Illinois Inst. of Technology (1987).

Aldis, D. F., and D. Gidaspow, "Two-Dimensional Analysis of a Dust Explosion," *AIChE J.*, **36**, 7 (1990).

Baer, M. R., and R. J. Gross, "A Two-Dimensional Flux-Corrected Transport Solver for Convectively Dominated Flows," Sandia Report SAND85-0613, Sandia National Lab. (1989).

Baer, M. R., J. W. Nunzaito, and P. F. Embid, "Deflagraton-to-Detonation Transition in Reactive Granular Materials," *Numerical Approaches to Combustion Modeling*, E. S. Oran and J. P. Boris, eds., 135, *Progress in Aeronautics and Astronautics*, AIAA, Washington, DC (1990).

Book, D. L., and M. A. Fry, "Airblast Simulations Using Flux-Corrected Transport Codes," Naval Research Laboratory Memorandum Report 5334, U.S. Naval Research Lab., Washington, DC, AD-A142 820 (1984).

Book, D. L., ed., "Flux Corrected Transport," *Finite-Difference Techniques for Vectorized Fluid Dynamics Calculations*, Chap. 3, Springer-Verlag, New York (1981).

Boris, J. P., and D. L. Book, "Flux-Corrected Transport: III. Minimal-Error FCT Algorithms," *J. of Comput. Phys.*, **20**, 397 (1976).

Chakravarthy, S. R., K. Y. Szema, U. C. Goldberg, and J. J. Gorski, "Applications of a New Class of High Accuracy TVD Schemes to the Navier-Stokes Equations," AIAA Paper 85-0165, Aerospace Sciences Meeting, Reno, NV (1985).

Chakravarthy, S. R., and S. Osher, "A New Class of High Accuracy TVD Schemes for Hyperbolic Conservation Laws," AIAA Paper 85-0363, Aerospace Sciences Meeting, Reno, NV (1985).

Cowperthwaite, M., and W. H. Zwisler, "TIGER Computer Program Documentation," Stanford Research Institute Project PYU-1182 for U.S. Army Picatinny Arsenal (Contract DAAA21-71-C-0454) and Stanford Research Project PYU-1281 for Lawrence Livermore Laboratory (Contract AT(04-3)-115) (1984).

Finlayson, B. A., *Numerical Methods for Problems with Moving Fronts*, Ravenna Park Publishing, Seattle (1992).

Gidaspow, D., *Multiphase Flow and Fluidization, Continuum and Kinetic Theory Descriptions*, Academic Press, San Diego (1994).

Gidaspow, D., and L. Huilin, "Collisional Viscosity of FCC Particles in a CFB," *AIChE J.*, **42**, 2503 (1996).

Gidaspow, D., M. Syamlal, J. L. Austing, A. J. Tulis, W. K. Sumida, and W. Comeyne, "The Large-Scale Detonation of a Particulate Pyrotechnic in a Computer-Modeled Dispersed State," Pyrotechnics Seminar (1984).

Godunov, S. K., A. V. Zabrodin, and G. P. Prokopov, "A Computational Scheme for Two-Dimensional Non Stationary Problems of Gas Dynamics and Calculation of the Flow From a Shock Wave Approaching a Stationary State," *Zh. uych. mat.*, **1**(6), 1020 (1961).

Gross, R. J., and M. R. Baer, "ETBFCT—A Solver for One-Dimensional Transport Equations," Sandia Report SAND85-1273 (1985).

Kunhardt, E. E., and C. Wu, "Towards a More Accurate Flux Corrected Transport Algorithm," *J. of Comput. Phys.*, **68**, 127 (1987).

Lyczkowski, R. W., D. Gidaspow, C. W. Solbrig, and E. D. Hughes, "Characteristics and Stability Analyses of Transient One-Dimensional Two-Phase Flow Equations and Their Finite Difference Approximations," *Nucl. Sci. and Eng.*, **66**, 378 (1978).

Miller, A., and D. Gidaspow, "Dense, Vertical Gas-Solid Flow in a Pipe," *AIChE J.*, **38**, 11 (1992).

Pape, R., "Multiphase Reactive Flow Modeling Applied to Dispersed Explosive Systems in a Detonation Tube," PhD Thesis, Illinois Inst. of Technology (1996).

Pape, R., D. Gidaspow, and S. Wu, "Multiphase Flow in Slurry Bubble Column Reactors and Solid Propellant Rockets," Int. Symp. on Numerical Methods for Multiphase Flows, ASME, San Diego, CA (1996a).

Pape, R., A. J. Tulis, D. Gidaspow, and W. Comeyne, "The Establishment of Stable Detonation Propagation in a Detonation Tube," Int. Pyrotechnics Symp., Fort Collins, CO (1996b).

Powers, J. M., D. S. Stewart, and H. Krier, "Theory of Two Phase Detonation: I. Modeling," *Combust. and Flame*, **80**, 264 (1990).

Powers, J. M., D. S. Stewart, and H. Krier, "Theory of Two Phase Detonation: II. Structure," *Combust. and Flame*, **80**, 264 (1990).

Richtmyer, R. D., and K. W. Morton, *Difference Methods for Initial Value Problems*, 2nd ed., Interscience Publishers, New York (1967).

Rivard, W. C., and M. D. Torrey, "K-FIX: A Computer Program for Transient Two-Dimensional, Two-Fluid Flow," Los Alamos, LA-NUREG-6623 (1977).

Smith, J. M., and H. C. Van Ness, *Introduction to Chemical Engineering Thermodynamics*, 4th ed., McGraw-Hill, New York (1987).

Sun, B., D. Gidaspow, R. Pape, and W. Comeyne, "The Numerical Modeling of a Dispersed Explosive System," Proc. Int. Pyrotechnics Seminar, Colorado Springs, CO (1994).

Tulis, A. J., and J. R. Selman, "Detonation Tube Studies of Aluminum Particles Dispersed in Air," Proc. Int. Symp. on Combustion, Haifa, Israel (1982).

Tulis, A. J., J. L. Austing, and D. C. Heberlein, "Detonation Tube Studies of Reactive Particles in Two-Phase Detonations," Proc. Int. Symp. on Shock Tubes and Waves, Sydney, Australia (1983).

Tulis, A. J., W. K. Sumida, and H. Egghart, "Detonation of Oxidizer Powders in Ethylene Gas," Proc. Int. Pyrotechnics Seminar, Boulder, CO (1990).

Tulis, A. J., W. K. Sumida, H. Egghart, and D. C. Heberlein, "Observations of Spinning Detonation in Two-Phase Fuel-Oxidizer Solids Dispersed in Gas One-Dimensional Tube Studies," Proc. Int. Pyrotechnics Seminar combined with Int. Symp. on Pyrotechnics and Explosives, Beijing, China (1991).

Tulis, A. J., and W. K. Sumida, "Detonation Tube Studies of Multi-Phase Dispersed Systems," IIT Research Institute Report No. IITRI-C06707-F, for U.S. Army Belvoir RD&E Center, Fort Belvoir, VA (1994).

Tulis, A. J., W. K. Sumida, R. P. Joyce, D. C. Heberlein and D. L. Patel, "Phenomenological Aspects in Explosive Powder/Gas Two-Phase Detonations," Int. Symp. on Combustion, Combustion Inst., Univ. of California, Irvine, CA, p. 79 (1994).

Van Leer, B., "Towards the Ultimate Conservation Difference Scheme. V. A Second-Order Sequel to Godunov's Method," *J. Comput. Physics*, **32**, 101 (1979).

Wu, S., and D. Gidaspow, "Simulation of Methanol Synthesis in G-L-S Slurry Bubble Column Reactors," *Chem. Eng. Sci.*, in press (1997).

Yee, H. C., "Linearized Form of Implicit TVD Schemes for the Mul-

tidimensional Euler and Navier-Stokes Equations," *Comput. & Math. with Appl.*, **12A**(4/5), 413 (1985).
Yee, H. C., "Construction of Explicit and Implicit Symmetric TVD Schemes and Their Applications," *J. Comput. Phys.*, **68**, 1 (1987).
Zha, G. C., and F. Bilgen, "Numerical Solutions of Euler Equations by Using a New Flux Vector Splitting Scheme," *Int. J. for Numerical Methods in Fluids*, **17**, 115 (1993).

Appendix: Frame Invariance of Momentum Relations

In this appendix, frame invariance is demonstrated for the momentum equations. The presentation given here is taken from the thesis of Pape (1996) and repeated for completeness. The primary purpose of this analysis is to assure that the form of the mass generation term in the gas-phase momentum equation satisfies the frame invariance requirement. Two approaches are taken. The first approach is direct application of the Galilean transformation to demonstrate that the equations are the same form regardless of the frame of reference. The second approach is converting the equations to the substantial derivative form to gain the perspective of viewing the system moving with the phase being evaluated.

The first approach taken here is implied but not detailed in the article by Powers et al. (1990). We consider only one dimension and Cartesian coordinates in this derivation. The Galilean transformation is applied to the equations

$$\xi = x - Dt \tag{A1}$$

Taking the derivative of ξ, we have

$$d\xi = dx - Ddt \tag{A2}$$

or

$$\frac{d\xi_f}{dt} = \frac{dx_f}{dt} - D \tag{A3}$$

$$\frac{d\xi_s}{dt} = \frac{dx_s}{dt} - D \tag{A4}$$

yielding

$$v_f = u_f - D \tag{A5}$$

$$v_s = u_s - D \tag{A6}$$

where v is velocity in the ξ frame of reference. Consider a general function ϕ for which we have

$$d\phi = \left.\frac{\partial\phi}{\partial x}\right|_t dx + \left.\frac{\partial\phi}{\partial t}\right|_x dt \tag{A7}$$

And applying Eq. A2

$$d\phi = \left.\frac{\partial\phi}{\partial x}\right|_t d\xi + \left(D\left.\frac{\partial\phi}{\partial x}\right|_t + \left.\frac{\partial\phi}{\partial t}\right|_x \right) dt \tag{A8}$$

Then, in turn, holding ξ and t constant, expressions for the partial derivatives are derived:

$$\left.\frac{\partial\phi}{\partial\xi}\right|_t = \left.\frac{\partial\phi}{\partial x}\right|_t \tag{A9}$$

$$\left.\frac{\partial\phi}{\partial t}\right|_x = \left.\frac{\partial\phi}{\partial t}\right|_\xi - D\left.\frac{\partial\phi}{\partial\xi}\right|_t \tag{A10}$$

These are the transformations needed to demonstrate frame invariance. Consider the continuity equation in generalized form given below

$$\left.\frac{\partial\mathfrak{J}}{\partial t}\right|_x + \left.\frac{\partial(\mathfrak{J}u)}{\partial x}\right|_t = \dot{m} \tag{A11}$$

where $\mathfrak{J}$ is bulk density of any phase k ($\epsilon_k \rho_k$), u is the velocity of phase k, and $\dot{m}$ is the mass generation rate of phase k. In order to prove frame invariance for the continuity equations, the above transformations are used, yielding the following derivation

$$\left.\frac{\partial\mathfrak{J}}{\partial t}\right|_\xi - D\left.\frac{\partial\mathfrak{J}}{\partial\xi}\right|_t + \mathfrak{J}\left.\frac{\partial v}{\partial\xi}\right|_t + v\left.\frac{\partial\mathfrak{J}}{\partial\xi}\right|_t + D\left.\frac{\partial\mathfrak{J}}{\partial\xi}\right|_t = \dot{m} \tag{A12}$$

$$\left.\frac{\partial\mathfrak{J}}{\partial t}\right|_\xi + \mathfrak{J}\left.\frac{\partial v}{\partial\xi}\right|_t + v\left.\frac{\partial\mathfrak{J}}{\partial\xi}\right|_t = \dot{m} \tag{A13}$$

and finally,

$$\left.\frac{\partial\mathfrak{J}}{\partial t}\right|_\xi + \left.\frac{\partial(\mathfrak{J}v)}{\partial\xi}\right|_t = \dot{m} \tag{A14}$$

This proves that the continuity equations are frame invariant.

Next, we prove frame invariance for the gas-phase momentum equation (the primary equation that is in question)

$$\mathfrak{J}\left.\frac{\partial u_f}{\partial t}\right|_x + \mathfrak{J}u_f\left.\frac{\partial u_f}{\partial x}\right|_t = \left.\frac{\partial P}{\partial x}\right|_t - \beta(u_f - u_s) + \dot{m}_f(u_s - u_f) \tag{A15}$$

The continuity equation in the x-frame of reference is multiplied by the gas velocity and then subtracted from the momentum equation

$$\mathfrak{J}\left.\frac{\partial u_f}{\partial t}\right|_x + u_f\left.\frac{\partial\mathfrak{J}}{\partial t}\right|_x + \mathfrak{J}u_f\left.\frac{\partial u_f}{\partial x}\right|_t + u_f\left.\frac{\partial\mathfrak{J}u_f}{\partial x}\right|_t - u_f\left.\frac{\partial\mathfrak{J}}{\partial t}\right|_x - u_f\left.\frac{\partial\mathfrak{J}u_f}{\partial x}\right|_t = \left.\frac{\partial P}{\partial x}\right|_t - \beta(u_f - u_s) + \dot{m}_f u_s - \dot{m}_f u_f \tag{A16}$$

This yields the nonconservative form of the momentum equation as follows:

$$\mathfrak{J}\left.\frac{\partial u_f}{\partial t}\right|_x + \mathfrak{J}u_f\left.\frac{\partial u_f}{\partial x}\right|_t = \left.\frac{\partial P}{\partial x}\right|_t - \beta(u_f - u_s) + \dot{m}_f(u_s - u_f) \tag{A17}$$

Equations A1, A9 and A10 are used to transform the gas momentum equation into the ξ frame of reference

$$\Im\left(\left.\frac{\partial(v_f+D)}{\partial t}\right|_{\xi}-D\left.\frac{\partial(v_f+D)}{\partial \xi}\right|_{t}\right)+\Im(v_f+D)\left.\frac{\partial(v_f+D)}{\partial \xi}\right|_{t}=\left.\frac{\partial P}{\partial \xi}\right|_{t}-\beta(v_f+D-v_s-D)+\dot{m}_f(v_s+D-v_f-D) \quad \text{(A18)}$$

Eliminating terms, it is shown that the form of the equation does not change in a Galilean transformation

$$\Im\left.\frac{\partial v_f}{\partial t}\right|_{\xi}+\Im v_f\left.\frac{\partial v_f}{\partial \xi}\right|_{t}=\left.\frac{\partial P}{\partial \xi}\right|_{t}-\beta(v_f-v_s)+\dot{m}_f(v_s-v_f) \quad \text{(A19)}$$

It is significant to note that as long as there is a term for the momentum contribution due to gas generation, the form of the source velocity in that term does not matter mathematically. There must be a term in the momentum equation $\dot{m}u_s$, or such a term will arise in the transformed equation and frame invariance will not be satisfied. However, as long as the term is present, the source velocity can be anything that is physically realistic, even zero if appropriate. In the case of a detonation propagation in a cloud of reactive particles, the solid particles are the source of gas generation in the gas phase. Therefore, physical reality corresponds to the gas products entering the system at the solids velocity. It is comforting that this situation is allowed by the frame invariance requirement.

Since, based on frame invariance, any physically realistic velocity can be used for the source term, we can define the following source velocity when there are multiple condensed phases

$$u_s=\frac{\sum_k \rho_k u_k}{\sum_k \rho_k} \quad \text{(A20)}$$

This is the source velocity used in the multiphase code evaluated in this article

The second approach is to convert the equations to the substantial derivative form. For this derivation, we keep the equations in general form with respect to the coordinate system and consider conservation of mass and momentum for the gas and a single solid phase, given in Eqs. A21–A24

$$\frac{\partial \epsilon_f \rho_f}{\partial t}+\nabla\left(\epsilon_f \rho_f \vec{v}_f\right)=\dot{m}_f=-\dot{m}_s \quad \text{(A21)}$$

$$\frac{\partial \epsilon_s \rho_s}{\partial t}+\nabla(\epsilon_s \rho_s \vec{v}_s)=\dot{m}_s=-\dot{m}_f \quad \text{(A22)}$$

$$\frac{\partial \epsilon_f \rho_f \vec{v}_f}{\partial t}+\nabla\left(\epsilon_f \rho_f \vec{v}_f \vec{v}_f\right)=\nabla \overline{\overline{T}}_f+\epsilon_f \rho_f \vec{f}_f+\hat{P}_f+\dot{m}_f \vec{v}_s \quad \text{(A23)}$$

$$\frac{\partial \epsilon_s \rho_s \vec{v}_s}{\partial t}+\nabla(\epsilon_s \rho_s \vec{v}_s \vec{v}_s)=\nabla \overline{\overline{T}}_s+\epsilon_s \rho_s \vec{f}_s+\hat{P}_s+\dot{m}_s \vec{v}_s \quad \text{(A24)}$$

Consider the solids momentum Eq. A24 first. This is expanded in Eq. A25, and then the conservation of mass for the solid phase (Eq. A22) is applied to obtain the substantial derivative form in Eq. A26.

$$\epsilon_s \rho_s \frac{\partial \vec{v}_s}{\partial t}+\vec{v}_s\left(\frac{\partial \epsilon_s \rho_s}{\partial t}+\nabla(\epsilon_s \rho_s \vec{v}_s)\right)+\epsilon_s \rho_s \vec{v}_s \nabla \vec{v}_s=\dot{m}_s \vec{v}_s+\nabla \overline{\overline{T}}_s+\epsilon_s \rho_s \vec{f}_s+\hat{P}_s \quad \text{(A25)}$$

$$\epsilon_s \rho_s \frac{d\vec{v}_s}{dt}=\nabla \overline{\overline{T}}_s+\epsilon_s \rho_s \vec{f}_s+\hat{P}_s \quad \text{(A26)}$$

For the fluid, the resultant form is the same as Eq. A26 with an additional term $\dot{m}_s(\vec{v}_s-\vec{v}_f)$ on the right. The additional term is invariant with respect to frame of reference due to the relative velocity.

Manuscript received May 27, 1997, and revision received Nov. 3, 1997.